Research Article

Feature Point Detection Utilizing the Empirical Mode Decomposition

Jesmin Farzana Khan,[1] Kenneth Barner,[2] and Reza Adhami[1]

[1] *Department of Electrical and Computer Engineering, University of Alabama in Huntsville, Huntsville, AL 35899, USA*
[2] *Department of Electrical and Computer Engineering, University of Delaware, Delaware, DE 19716, USA*

Correspondence should be addressed to Jesmin Farzana Khan, khanj@eng.uah.edu

This paper introduces a novel contour-based method for detecting largely affine invariant interest or feature points. In the first step, image edges are detected by morphological operators, followed by edge thinning. In the second step, corner or feature points are identified based on the local curvature of the edges. The main contribution of this work is the selection of good discriminative feature points from the thinned edges based on the 1D empirical mode decomposition (EMD). Simulation results compare the proposed method with five existing approaches that yield good results. The suggested contour-based technique detects almost all the true feature points of an image. Repeatability rate, which evaluates the geometric stability under different transformations, is employed as the performance evaluation criterion. The results show that the performance of the proposed method compares favorably against the existing well-known methods.

1. INTRODUCTION

There are a wide variety of methods reported in the literature for interest point and corner detection in grey-level images. Current detection methods can be categorized into three types: contour-based, parametric model-based, and intensity-based methods. Contour-based methods first extract contours and then search for maximal curvature or inflexion points along the contour chains, or carry out some polygonal approximation and then search for intersection points. Contour-based methods have existed for some time [1–6]. This work proposes a contour-based technique that is inspired by the fact that there is a correspondence between the wavelet decomposition and the EMD of a given signal, for example, the wavelet decomposition of a signal gives higher energy where the signal contains information, while the intrinsic mode function (IMF) of the EMD shows higher frequency content at the same locations. Corner detection schemes using the wavelet transform (WT) are popular due to the fact that the WT is able to decompose an input signal into smooth and detailed parts by low-pass and high-pass filters at multiresolution levels [7]. In this manner, local deviations are easily captured at various detailed decompo-

sition levels. Several wavelet-based approaches are reported in [8–15].

Parametric model methods fit a parametric intensity model to the signal. They often provide subpixel accuracy, but are limited to specific types of interest points, for example, L-corners. A parametric model is used in [16–19]. Intensity-based methods compute a measure that indicates the presence of an interest point directly from the grey values. This type of detector does not depend on edge detection or mathematical models [20–30].

This paper presents a novel contour-based interest point detector, which is largely affine transformation invariant. The main contribution of this work is the introduction of the 1D EMD [31] for extracting feature points from edges. In addition, a new scheme for edge thinning is proposed. Specifically, edge detection is performed using morphological gradient operator [32], followed by edge thinning based on edge thickness in the horizontal and vertical directions. To detect true corner points from the circular arcs, the 2D boundaries of an object are represented by the 1D tangent angles of the boundary point coordinates. Then eigenvectors of the covariance matrix of the coordinates are calculated over a small boundary segment [15, 33]. Based on the fact

that true corners result in stronger tangent variations, the 1D EMD is utilized to decompose the 1D tangent angles and capture the irregular angle variations. Finally, the locations of the true feature points are identified by comparing the local frequency content of the first intrinsic mode function (IMF) of the 1D decomposed signal with a predefined threshold.

A requirement for good feature point detection is that the detector be invariant to image transformations and yields the same detected points for different viewpoints. The proposed method is largely invariant to significant affine transformations including large rotations and scale changes. Such transformations introduce significant changes in point locations as well as in the scale and the shape of the neighborhoods of interest points. Our approach addresses these problems simultaneously and offers invariance to geometric transformation. Thus, the points detected in the original image and points detected after the transformation of the image commute. Such points have often been called invariant feature points in the literature, though in principle they change covariantly with the transformation. Thus, even though the regions themselves are covariant, the normalized image pattern they cover and the feature descriptors derived from them are typically invariant.

In this paper, we evaluate the proposed method utilizing the "repeatability" [34] criteria, which directly measures the quality of the detected feature points for tasks such as image matching, object recognition, and 3D reconstruction. It is complementary to localization accuracy, which is relevant for tasks such as camera calibration and 3D reconstruction of specific scene points. Repeatability and localization are conflicting criteria; smoothing improves repeatability but degrades localization [35]. Repeatability explicitly compares the geometrical stability of the detected interest points between different images of a given scene taken under varying viewing conditions. An interest point is "repeated" if the 3D scene point detected in the first image is also accurately detected in the transformed image. The proposed detector is compared to five existing methods that have been shown to yield good results. Utilizing repeatability, the proposed method is shown to yield comparable to improved results.

The remainder of the paper is organized as follows: the proposed corner detection algorithm is described in Section 2. Experimental results along with the comparison to five other existing methods are demonstrated in Section 3. Concluding remarks and recommendations for future improvement are given in Section 4.

2. PROPOSED ALGORITHM

2.1. Motivation

It is reported that the wavelet transform is a robust scheme for feature points detection due to its ability to decompose an input signal into smooth and detailed components. This fact motivates the consideration of the EMD for interest. The EMD technique was developed recently to analyze the time-frequency distribution of nonlinear and nonstationary data. The EMD is an adaptive decomposition through which any
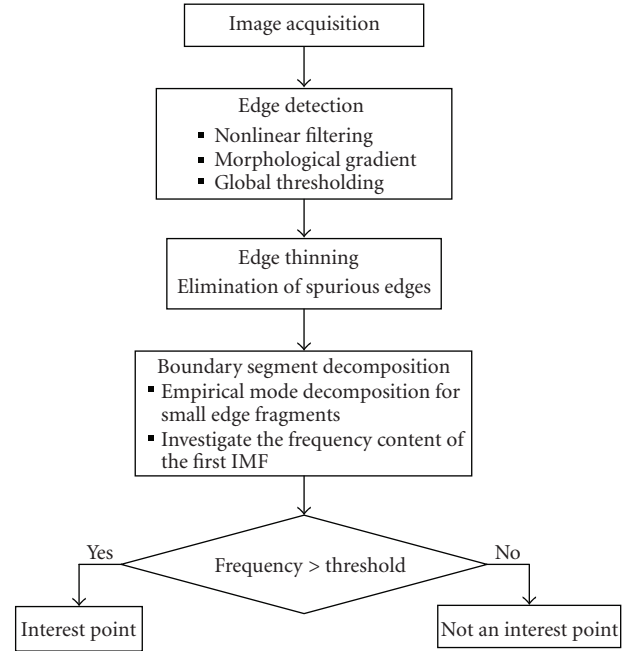

FIGURE 1: Block diagram of the proposed algorithm.

signal can be decomposed into its IMFs that provide well-defined instantaneous frequency information of the signal.

Unlike Fourier or wavelet techniques, the EMD does not assume the form of the underlying oscillatory modes or basis functions. For a given signal, the wavelet decomposition is less compact and physically meaningful than the EMD results [36]. The EMD decomposition method is adaptive and highly efficient. Since the decomposition is based on the local characteristic of the data, it is applicable to nonlinear and nonstationary processes. Experimental results presented here show that, for feature point selection, the EMD is also robust and gives better performance than wavelet approaches.

In the proposed approach, we select the feature points from the edges and, to make the selection process robust, we use morphological edge detection along with edge thinning. The methodology of the proposed method is to use an eigenvector of the covariance matrix for a boundary point over a small region of support (ROS) on a small boundary segment as a curvature function for feature point detection. Thus, we perform the EMD on small edge fragment after edge detection and thinning operations. The derived edge detection and thinning method is used in lieu of traditional method, such as Canny edge detection [35], because it returns edge segments rather than contiguous edge lines, which is beneficial in feature point detection.

2.2. The EMD-based feature point determination

A block diagram of the proposed algorithm is shown in Figure 1, and the algorithm steps are summarized as follows.

After acquiring the image, edge detection is performed based on mathematical morphology [32] applied to the intensity image. The intensity image is first blurred by

open-close and close-open filters [37]. Next, a morphological gradient operator is applied to the blurred image, which gives symmetric edges between foreground and background regions, and the resulting image is converted to binary edge map by a global nonhistogram-based thresholding technique [38]. A new edge thinning algorithm is applied to this binary image to obtain fine, narrow, and well-defined object boundaries. Next, a novel technique for selecting feature points from object boundaries based on the EMD is employed. In this work, we represent edges as a set of straight or curved line fragments that are used to extract local curvature by analyzing the eigenvectors of covariance matrices using the 1D EMD. Specifically, each small 2D boundary segment is transformed to a 1D $\theta - P$ representation (where θ is the tangent angle variations of the arc length, P, along the object's boundary) that is decomposed using the 1D EMD. At the true feature points, the first IMF signal of the EMD shows distinctly higher frequency contents than at the points which carry less, or no, information. Thus, points where the frequency measure of the first IMF signal is greater than a predefined threshold are set as interest points. The following subsections discuss each step of the algorithm in detail.

2.2.1. Morphological edge detection

Most classical edge detectors such as Laplacian of Gaussian (LoG) [39] and Canny [35] are based on differential operations and hence are primarily effective in detecting step edge. In contrast to classical techniques, morphological operations [37] are highly effective in detecting different types of features. In this paper, a morphological scanning edge detector (MSED) [32] is applied. The operator is insensitive to skew and orientation, free from artifacts introduced by both global and fixed size block-based local thresholding, and robust to noise. It has been reported that edge features [40] can better handle lighting and scale variations in natural scene images than texture features [41, 42]; therefore, we choose to use an edge-based approach in this study.

An efficient morphological edge detection scheme is applied to the the intensity image, I, as follows [32]. The image I is first blurred (to reduce false edges and oversegmentation) using open-close and close-open filters [37]. The final blurred image, I_b, is the average of the outputs of these two filters,

$$I_b = \frac{{}_B({}_B I_o)_c + {}_B({}_B I_c)_o}{2}, \tag{1}$$

where B is the 3×3 eight-connected structuring element, and ${}_B I_o$ and ${}_B I_c$ denote the opening and closing of I by the structuring element B, respectively. Next, the morphological gradient operator [43] is applied to the blurred image I_b, resulting in an image,

$$I_{es} = \delta^B(I_b) - \varepsilon^B(I_b), \tag{2}$$

where δ^B and ε^B and are the dilation and erosion operators, respectively, utilizing the 3×3 eight-connected structuring element B. The morphological gradient is an edge-strength

extraction operator that gives symmetric edges between the foreground and background regions. The resulting image, I_{es}, is then thresholded to obtain a binary edge mask. A global nonhistogram-based thresholding technique is incorporated rather than local (adaptive) thresholding [38]. The threshold level, γ, is set as,

$$\gamma = \frac{\sum (I_{es} \cdot c)}{\sum c}, \tag{3}$$

where $\cdot$ denotes pixel-wise multiplication and $c = \max(|g_1 * * I_{es}|, |g_2 * * I_{es}|)$; also $g_1 = [-1 0 1]$; $g_2 = [-1 0 1]^T$, and $**$ denotes 2D linear convolution. The binary edge image I_e is then given by,

$$I_e = \begin{cases} 1 & \text{if } I_{es} > \gamma, \\ 0 & \text{otherwise.} \end{cases} \tag{4}$$

To thin the edges, the morphological edge map is scanned along the horizontal and vertical directions to reduce the width of the edges to a single pixel by through erosion. During horizontal scanning, all the nonzero neighborhood pixels of a nonzero edge pixel in a horizontal window $1 \times w_h$ are set to 0. The resulting image is I_{he},

$$\text{if } I_e(x_i, y_j) \neq 0,$$
$$\text{then } \begin{cases} I_{he}(x_i, y_j) = I_e(x_i, y_j) \\ \\ I_{he}(x_i, y_k) = 0; \quad \text{for } k \in_{k \neq j} \left\{ j - \frac{w_h}{2}, \ j + \frac{w_h}{2} \right\}. \end{cases} \tag{5}$$

Similar operations in the vertical direction yield

$$\text{if } I_e(x_i, y_j) \neq 0,$$
$$\text{then } \begin{cases} I_{he}(x_i, y_j) = I_e(x_i, y_j) \\ \\ I_{he}(x_i, y_k) = 0; \quad \text{for } k \in_{k \neq j} \left\{ j - \frac{w_h}{2}, \ j + \frac{w_h}{2} \right\}. \end{cases} \tag{6}$$

The maximum of I_{he} and I_{ve} is set as the thinned binary edge image, I_{te}, resulting from the edge thinning operation, $I_{te} = \max(I_{he}, I_{ve})$. The image I_{te} may still contain isolated noisy spurious edges. To remove these edge, segments of length less than N are deleted. Let n sequential points describe an edge segment P in I_{te} such that $P = \{p_i = (x_i, y_i); i = 1, 2, 3 \cdots n\}$. Then

$$I_{te}(x_i, y_i) = 0 \quad \text{for } (x_i, y_i) \in P, \ n \leq N. \tag{7}$$

The resulting final binary edge image, I_{fte}, contains 1pixel width boundaries in the image.

As an example, the intensity image, the morphological edge strength extracted image, gradient image after global thresholding, and the final edge image after thinning and elimination spurious edges are shown in Figures 2(a), 2(b), 2(c), and 2(d), respectively.
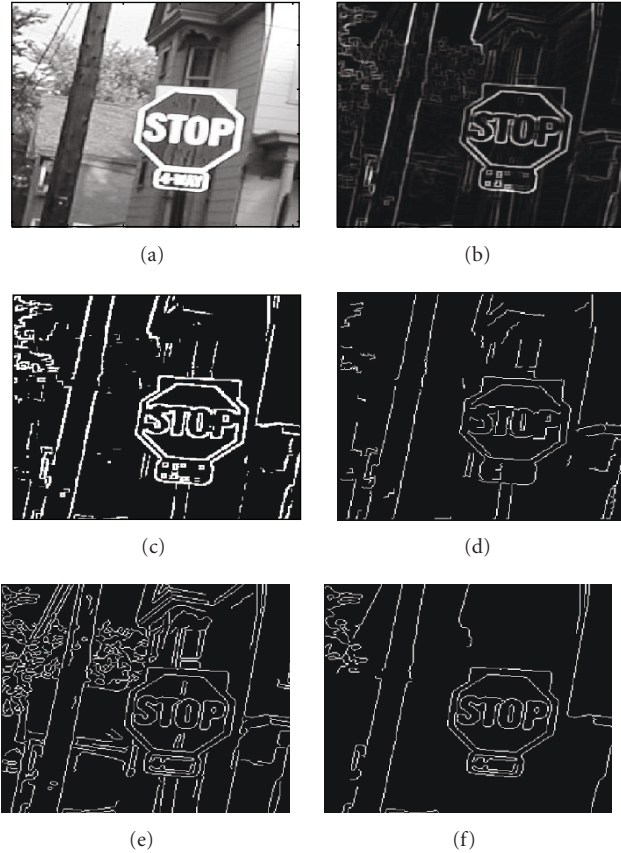
FIGURE 2: (a) Intensity image, (b) morphological edge strength image, (c) morphological edge after thresholding, (d) final edge image after thinning, (e) Canny edge image for a low threshold and (f) Canny edge image for a high threshold.

The reason for not using an existing edge detection method, for example, Canny edge detection method [35], is that Canny's method yields extraneous boundaries as shown in Figure 2(e). Though for a higher threshold Canny method gives fewer boundaries. In using this approach, however, the threshold needs to be determined by hand for each image. Moreover, even by setting a different threshold it does not return edge segments but rather long continuous edges and connected edges between two objects. The methodology of the proposed algorithm is to use the covariance matrix for a boundary point over a small region of support (ROS), on a small boundary segment, as a curvature function for feature point detection. It has been found that the morphological framework and edge thinning scheme yields edge segments, which facilitates the extraction of feature points.

2.2.2. Empirical mode decomposition

The EMD decomposes a signal into a finite number of (zero mean) frequency and amplitude modulated signals called IMFs. The first IMF contains the highest local frequencies of oscillation while the final IMF, or the residue, contains a single extremum, a monotonic trend, or simply a constant.

The basic idea embodied in the EMD analysis, as introduced by Huang et al. [31], is to allow for an adaptive and unsupervised representation of the intrinsic components of linear and nonlinear signals, based purely on the properties observed in the data without appealing to the concept of stationarity. Although the EMD is a relatively new data analysis technique, its power and simplicity have encouraged its application in a myriad of fields, including almost all areas of signal processing, image processing, computer vision, and medical analysis [44–48].

2.2.3. Feature points extraction

After obtaining the binary edge image, I_{fte}, the feature points along the boundaries of objects must be determined. If the boundary of an object involves both straight lines and circular arcs, spurious corners may be detected at circular arcs by boundary-based approaches. To overcome this shortcoming, Tsai et al. [33] introduced the eigenvalues of a covariance matrix for a boundary point, over a small region of support (ROS) on a small boundary segment, as a curvature function for feature point detection. We adopt this approach in order to retain the robust merits of covariance matrix in feature point detection. However, instead of using multiple eigenvalues, the principal eigenvector is used in this work, because the dominant orientation of any pixel in the local neighborhood can be either denoted as the argument of the principal eigenvector or by using the ratio between two eigenvalues. This technique is applied to each segment of the 2D boundaries of the edge image and feature points are extracted from each segment. As this approach considers a small boundary segment as a new curvature function for feature detection, image noise and quantization effect are readily eliminated.

The 1D wavelet transform has been utilized as a robust scheme in feature point detection due to its excellent local deviations capturing capability. In this work, the 2D boundaries of an object are initially transformed to a 1D $\theta - P$ representation. Then, 1D $\theta - P$ signal is used as input for the 1D EMD to detect the local deviations as measured by the number of zero crossing points of the first IMF. In the following, we present the procedure of finding the tangent angle of the boundary point.

2.2.4. 1D $\theta - p$ representation of boundary segment

From the binary edge image, I_{fte} the x-y coordinates of each point of a boundary segment of an object are first extracted into an array. Let a boundary P of an object be described by n sequential digital points, $P = \{p_i = (x_i, y_i); i = 1, 2, 3 \cdots n\}$, where p_{i+1} is adjacent to p_i on P. Let $N_s(p_i)$ denote a small boundary segment of P with point p_i is at the center of $N_s(p_i)$ over the ROS between points p_{i-s} and p_{i+s} for some integer s. That is, $N_s(p_i) = \{p_j : j \in \{i - s, i + s\}\}$. Therefore, the covariance matrix $M(p_i)$ for point p_i is estimated by the boundary points coordinates within $N_s(p_i)$ [49];

$$M(p_i) = \begin{bmatrix} m_{11} & m_{12} \\ m_{21} & m_{22} \end{bmatrix}, \tag{8}$$

where,

$$m_{11} = \left[\frac{1}{2s+1} \sum_{j=i-s}^{j=i+s} x_j^2 \right] - \bar{x}_i^2,$$

$$m_{22} = \left[\frac{1}{2s+1} \sum_{j=i-s}^{j=i+s} y_j^2 \right] - \bar{y}_i^2,$$

$$m_{12} = m_{21} = \left[\frac{1}{2s+1} \sum_{j=i-s}^{j=i+s} x_j y_j \right] - \bar{x}_i \bar{y}_i, \qquad (9)$$

$$\bar{x}_i = \frac{1}{2s+1} \sum_{j=i-s}^{j=i+s} x_j,$$

$$\bar{y}_i = \frac{1}{2s+1} \sum_{j=i-s}^{j=i+s} y_j,$$

where $\bar{x}_i$ and $\bar{y}_i$ are the geometrical center of $N_s(p_i)$. The covariance matrix $M(p_i)$ is a 2×2 symmetric, positive semidefinite matrix. The eigenvalues λ_1 and λ_2 of $M(p_i)$ are the solutions of the characteristic equation $\text{DET}(M(p_i) - D)$, where D is unit matrix. The corresponding eigenvectors E_1 and E_2 represent the tangent (major axis) and the normal (minor axis) directions for point p_i over the segment $N_s(p_i)$, respectively. Therefore, the tangent angle of point p_i, denoted by $\theta(p_i)$, is simply defined as follows:

$$\tan\theta(p_i) = \frac{(\lambda_1 - m_{11})}{m_{12}},$$
$$\theta(p_i) = \arctan\left(\frac{\lambda_1 - m_{11}}{m_{12}} \right). \qquad (10)$$

In general, the magnitude of $\theta(p_i)$ is between $-\pi/2$ and $\pi/2$. However, in order to avoid the large variation for two adjacent boundary points due to quantization effects [8, 10], $\theta(p_i)$ is defined as between 0 and $\pi/2$. That is, $\theta(p_i) = |\arctan((\lambda_1 - m_{11})/m_{12})|$. However, if m_{12} equals to 0, then $\theta(p_i)$ is set to $\pi/2$ to avoid divided by zero situations. Therefore, the angle of a boundary point p_i can be calculated by the eigenvector E_1 of $M(p_i)$ and the above expression for $\theta(p_i)$.

2.2.5. Detection procedure

Consider an n_1-point digital boundary, $P = \{ p_i = (x_i, y_i); i = 1, 2, 3 \cdots n_1 \}$, traversing points $(x_1, y_1), (x_2, y_2), \ldots, (x_{n_1}, y_{n_1})$, and circumventing the boundary in the counterclockwise direction. For each p_i sequence, there corresponds a 1D $\theta - P$ signal, $\theta(p_i)$, 1D wavelet signal, $Y(p_i)$, and a 1D first IMF signal of the EMD, $X(p_i)$.

As an example, we have chosen a binary image with one object. Figure 3(a) shows a binary image of an artificial "h"-shape object. Figure 3(b) presents the edge image of that object with one boundary involving $n_1 = 273$ boundary points. The character "+" in Figure 3(b) denotes the starting boundary point (x_1, y_1) and the arrow indicates the direction of boundary following. The corresponding 1D $\theta - P$ representation of the object boundary, $\theta(p_i)$ is shown at the top of Figure 3(c), which is used as an input signal to both the
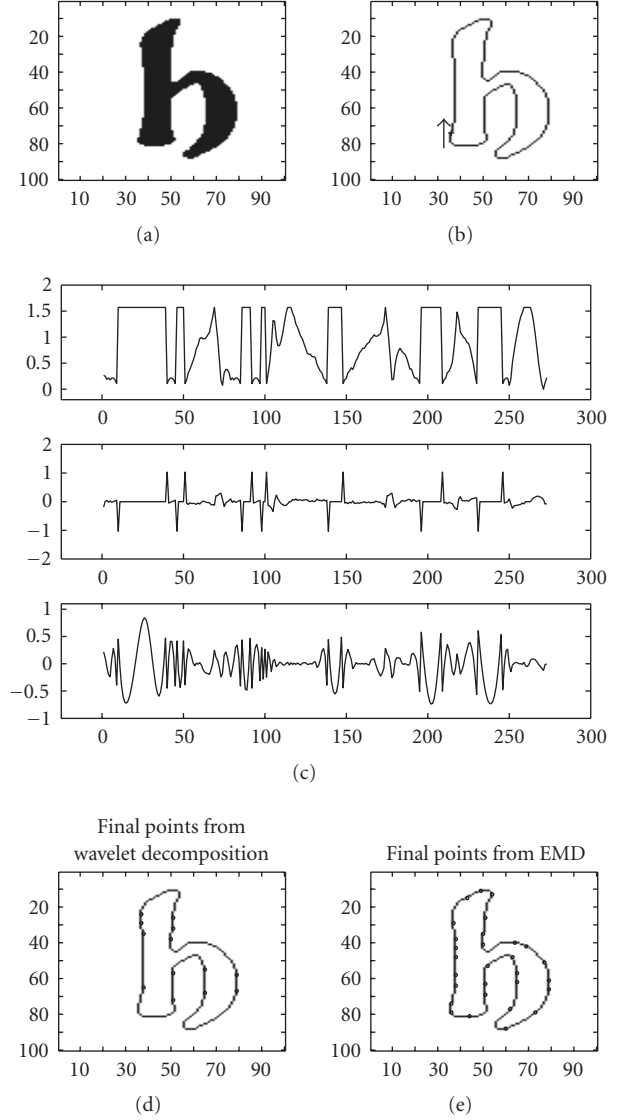

FIGURE 3: (a) Binary image of letter "h"; (b) starting boundary point and direction of boundary following; (c) the 1D $\theta - P$ representation of the "h"-shape object (top), haar wavelet decomposition at first decomposition level (middle), and the first IMF of the EMD (bottom); (d) feature points obtained from the location of distinct wavelet coefficients; and (e) feature points obtained from the frequency content of the first IMF of the EMD.

1D wavelet decomposition utilizing the "harr" basis function and the 1D empirical mode decomposition. The middle plot of Figure 3(c) shows 1D wavelet coefficients at the finest (first) detailed decomposition level, $Y(p_i)$. The bottom plot of Figure 3(c) is the first IMF $X(p_i)$ obtained from $\theta(p_i)$. The correspondence between the wavelet decomposition and the first IMF of the EMD for the 1D input signal can clearly be observed from Figure 3(c). Both the wavelet coefficients and the frequency of the first IMF are distinctly higher at the same points of that original 1D signal. The finest scale wavelet energies are distinctly higher at the true feature points than at the smooth regions. Feature points extracted from the binary

image of letter "h" based on the 1D wavelet decomposition method are shown in Figure 3(d).

In the EMD case, the first IMF shows distinctly higher frequency content at true feature points than at straight lines. The algorithm for finding true interest points makes four passes through the IMF signal. First, points are selected if they exceed a minimum number of zero crossings around them. Second, if two selected points are adjacent then one is deleted based on the concentration of zero crossings. During the third pass, the selected points that are not locally maximum in the original intensity image in its 3×3 neighborhood are deleted. In the final pass, the subset of pixels are kept such that the minimum distance between any pair of points is larger than a given threshold.

Let $Z(p_i)$ be the set of zero-crossing points of the IMF around p_i:

$$
\begin{aligned}
Z(p_i) = \{ p_j : X(p_{j-1})X(p_{j+1}) < 0 \}; \\
\text{for } j \in \left\{ i - \frac{W_z}{2}, i + \frac{W_z}{2} \right\},
\end{aligned}
\tag{11}
$$

where W_z defines window centered at p_i. If for a point, the number of zero crossings is greater than a predefined threshold, th_z (in our work, the threshold is 1/3 of the maximum number of zero crossings in the IMF signal), that point is likely a feature point. This is the first selection of the feature points from the object boundary, which forms the set $F_1 \subset P$:

$$
\begin{aligned}
F_1 &= \{ p_i : Z(p_i) > \text{th}_z \} \\
&= \{ p_i = (x_i, y_i); i = 1, 2, 3, \cdots, n_2 : n_2 < n_1 \},
\end{aligned}
\tag{12}
$$

where n_1 is the number of all the boundary points and n_2 is the number of selected points after discarding redundant points.

To discard redundant points, we check whether several neighboring points have the same number of zero-crossing points over a $W_s = 1 \times 11$ size window, and we keep the points among those that have the most concentrated zero-crossing points. Hence for each point over the window W_z, we calculate the sum of the distances from all the zero-crossing points to the point under consideration, p_i,

$$
S(p_i) = \sum_{j=i-W_z/2}^{j=i+W_z/2} |p_i - p_j|.
\tag{13}
$$

If $F_2 \subset F_1$ is the set of feature points after discarding redundant points from F_1, then $\overline{F_2} \cap F_1$ is the set of discarded points:

$$
\begin{aligned}
\overline{F_2} \cap F_1 &= \{ p_j : Z(p_j) = Z(p_i) \text{ and } S(p_j) \neq \min\{S(p_j)\} \} \\
&\qquad \text{for } j \in \left\{ i - \frac{W_s}{2}, i + \frac{W_s}{2} \right\}, \\
F_2 &= \{ p_i = (x_i, y_i); i = 1, 2, 3, \cdots, n_3 : n_3 < n_2 < n_1 \},
\end{aligned}
\tag{14}
$$

where n_3 is the number of selected points after discarding redundant points from F_1.

Figure 4: A synthetic image.

Finally, from the points in F_2, we retain those points that are locally maximum in their $W_m = 3 \times 3$ neighborhood with the restriction that the distance between any two feature points is larger than a given threshold (this is set to 5 pixels in our experiment). Thus, $F_3 \subset F_2$ is the set of feature points that are locally maximum in the edge image, I_{fte}, and $F_f \subset F_3$ is the final set of feature points after discarding those closely spaced points:

$$
\begin{aligned}
F_3 &= \left\{ p_i = (x_i, y_i) : I_{\text{fte}}(x_i, y_i) = \max_{\{j \in i - W_m/2, i + W_m/2\}} I_{\text{fte}}(x_j, y_j) \right\}, \\
F_3 &= \{ p_i = (x_i, y_i); i = 1, 2, 3 \cdots n_4 : n_4 < n_3 < n_2 < n_1 \},
\end{aligned}
\tag{15}
$$

where n_4 is the number of selected points after discarding redundant points from F_2:

$$
\begin{aligned}
F_f &= \{ p_i : |p_i - p_{i-1}| > 5 \text{ pixels, and } |p_i - p_{i+1}| > 5 \text{ pixels} \}, \\
F_f &= \{ p_i = (x_i, y_i); i = 1, 2, 3 \cdots n_5 : n_5 < n_4 < n_3 < n_2 < n_1 \},
\end{aligned}
\tag{16}
$$

where n_5 is the number of selected points after discarding redundant points from F_3.

Following the above procedure, the extracted final feature points, F_f for the artificial "h"-shape object are shown in Figure 3(e). By comparing the final feature point extraction results shown in Figures 3(d) and 3(e), it can be said that the IMF is richer in containing useful information about the original signal than the wavelet decomposition. That is, the EMD determined feature points are found at all the curvatures of the object whereas the wavelet decomposition approach misses some curvatures.

For an image with more than one object and objects with complicated shape, we perform the EMD on each edge fragment to extract local curvature following the above procedure. Thus, we find feature points for each fragment of edge independently and the final feature points are the accumulation of all the points obtained from all the edge boundary segments.

3. EXPERIMENTAL RESULTS

Results of experiments conducted to test the efficacy of the proposed corner detection algorithm are provided. In order to test the immunity of the proposed algorithm to
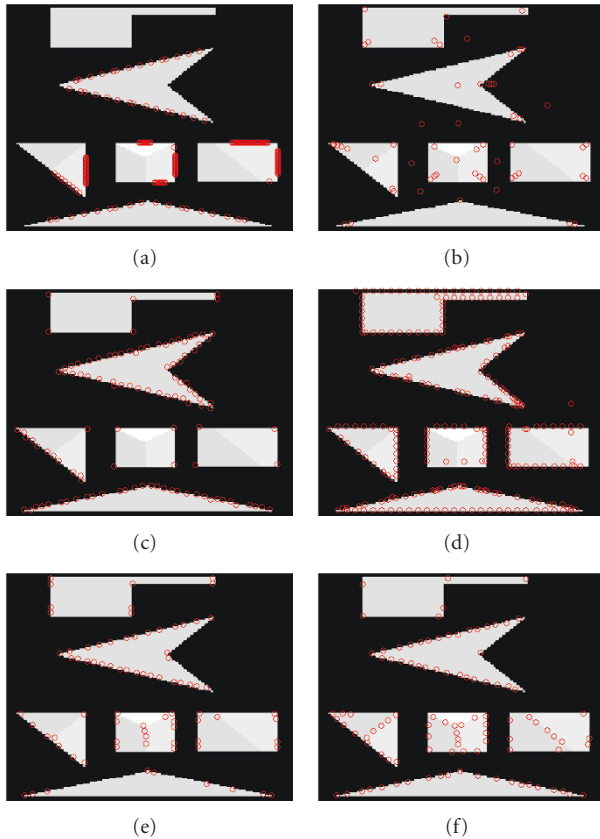
(a)

(b)

(c)

(d)

(e)

(f)

FIGURE 5: Feature points detected in the synthetic image by (a) Harris method (b) Lowe's method, (c) Tomasi's method, (d) Loupias's technique, (e) Yeh's algorithm, and (f) proposed technique.
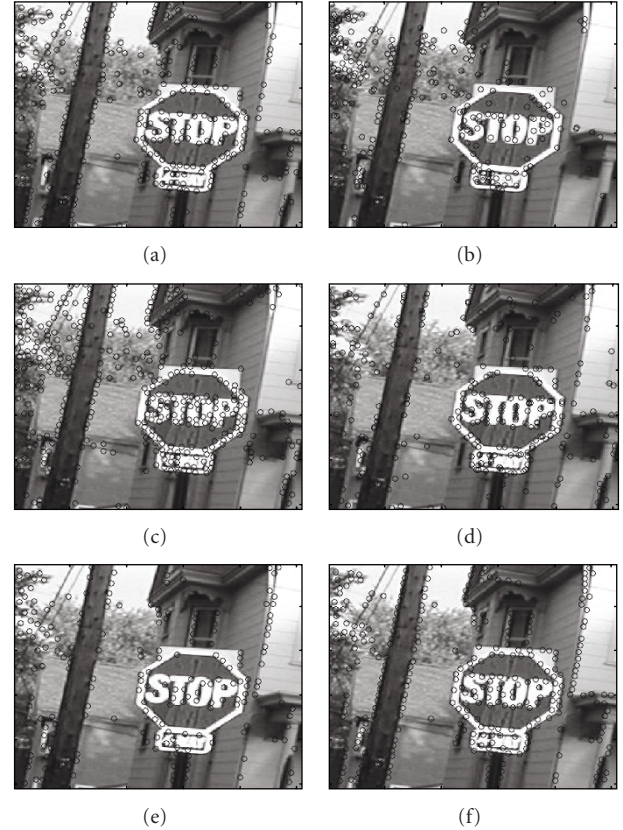
FIGURE 6: Feature points detected by (a) Harris method (b) Lowe's method, (c) Tomasi's method, (d) Loupias's technique, (e) Yeh's algorithm, and (f) proposed technique.

transformations, the original images are scaled, rotated, and sheared. Stability to image noise is also tested. Additionally, the repeatability rates of five interest point detectors are compared with the presented method under different image rotation and scale changes. Finally, analysis is performed on parameter sensitivity of the algorithm.

For comparison, we have chosen five detectors that are reported to offer good performance. Among the five chosen detectors, Harris's [24], Lowe's [30], and Tomasi's methods [25] are intensity-based methods. These are chosen because Harris's method has been reported to be better than any other detector, Lowe's algorithm also known as SIFT (scale invariant feature transform) is the best scale invariant detector, and Tomasi's detector is the best for tracking applications. The other two detectors [13, 15] are chosen because (1) they are contour-based methods like the proposed method and (2) they use the wavelet decomposition.

The above mentioned methods and the proposed algorithm are first applied to a synthetic image consisting of horizontal, vertical, and slanted lines; and different types of corners. As shown in Figure 4, this synthetic image contains both prominent and faint edges. The feature points detected by Harris's, Lowe's, Tomasi's, Loupias's, and

Yeh's methods are shown in Figures 5(a), 5(b), 5(c), 5(d), and 5(e), respectively. The interest points extracted by the presented algorithm are given in Figure 5(f). Even though the proposed method identifies fewer number of feature points than some of the presented approaches, it is interesting to observe that these feature points are distributed along all edges, boundaries, and corners of interest. This is true for prominent boundaries and edges, as well as subtle interior edges. Many object corners and boundaries are missed by the other methods, especially the faint interior edges. Thus, the proposed method has produced the most judicious feature points, placing them logically along the structures of interest.

Simulation results for the five methods on a real image are presented in Figure 6. For the reference image shown in Figure 2(a), feature points extracted by Harris's approach, Lowe's procedure, Tomasi's method, Loupias's technique, and Yeh's algorithm are shown in Figures 6(a), 6(b), 6(c), 6(d), and 6(e), respectively. The points detected by the presented method are given in Figure 6(f). From this figure, it can be seen that points selected by the proposed method cover all the curvatures of object boundaries and yields the most true corner points.

To evaluate detector rotation invariance, Figures 7 and 8 show the detection results for two rotated versions of
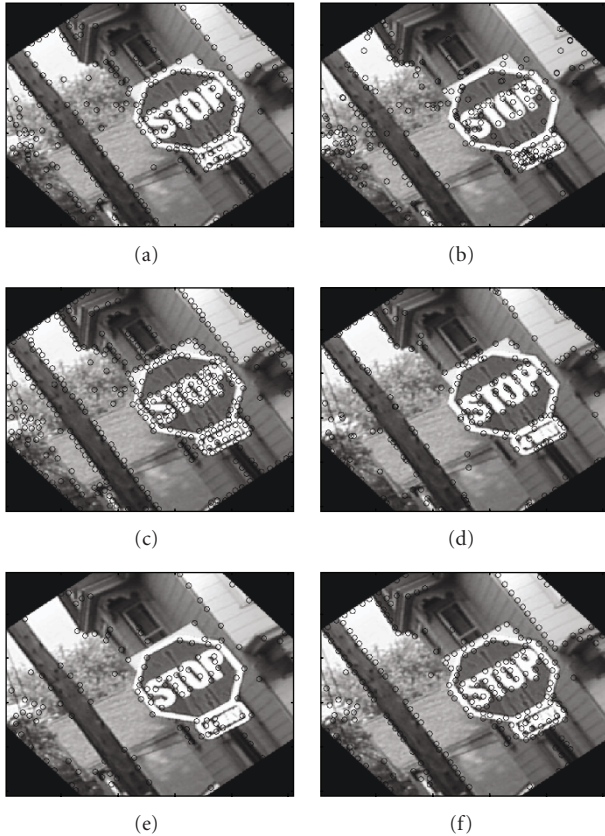
Figure 7: Feature points detected in 40° rotated image by (a) Harris method (b) Lowe's method, (c) Tomasi's method, (d) Loupias's technique, (e) Yeh's algorithm, and (f) proposed technique.

Figure 8: Feature points detected in 110° rotated image by (a) Harris method (b) Lowe's method, (c) Tomasi's method, (d) Loupias's technique, (e) Yeh's algorithm, and (f) proposed technique.

the reference image. Figures 7(f) and 8(f) give the results of the proposed method, where the rotation angle for the images are 40° and 110° for the images in Figures 7 and 8, respectively. The performance of Harris's, Lowe's, Tomasi's, Loupias's, and Yeh's methods are given in Figures 7(a), 7(b), 7(c), 7(d), and 7(e), respectively, for 40° rotation and in Figures 8(a), 8(b), 8(c), 8(d), and 8(e), for 110° rotation. From the figures, it is observed that Harris's, Lowe's, and the proposed method give the best result for both rotations. The performance of Tomasi's technique is better than Loupias's and Yeh's methods.

The effect of image scale change on detection result is tested and demonstrated in Figures 9 and 10. The points detected by the proposed technique are shown in Figures 9(f) and 10(f), where the scale changes are 1.5 and 3.4, respectively. Points detected by Harris's, Lowe's, Tomasi's, Loupias's, and Yeh's methods are presented in Figures 9(a), 9(b), 9(c), 9(d), and 9(e), respectively for the scale change 1.5 and in Figures 10(a), 10(b), 10(c), 10(d), and 10(e), respectively for the scale change 3.4. It can be seen from the figures that all the methods are scale invariant.

To evaluate the functioning of all five detectors as affine invariant systems, nonuniform scaling is applied in some directions to have shearing in the reference image shown in
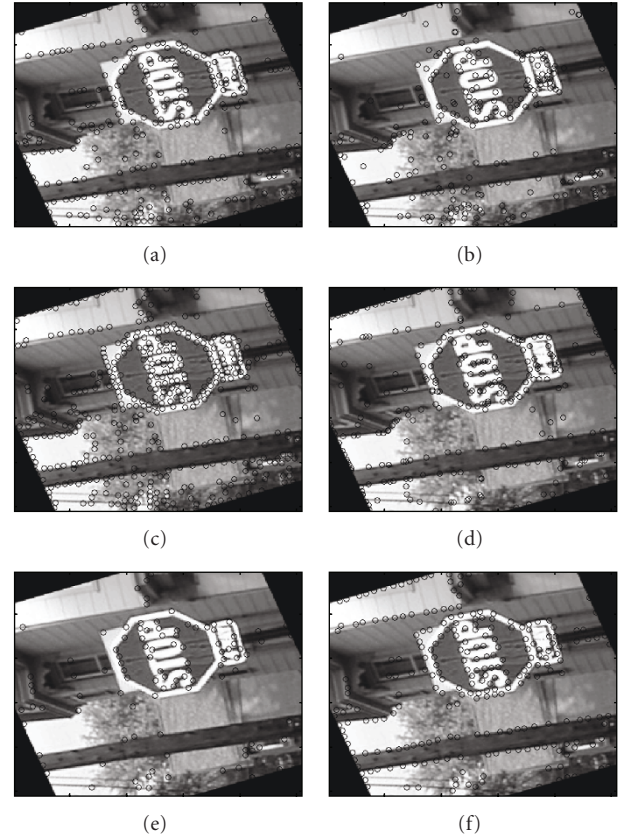
Figure 2(a). Figure 11(f) displays the feature points detected in the sheared image by the proposed method. The results of detection by Harris's, Lowe's, Tomasi's, Loupias's, and Yeh's methods are presented in Figures 11(a), 11(b), 11(c), 11(d), and 11(e), respectively. By examining the figure, it can be said that the proposed method performs satisfactorily for detecting interest points from the sheared image as well.

To check the performance with noise, we have added Gaussian noise to the original image. For a noisy image with a SNR of 25 dB, Figure 12(f) presents the points detected by the proposed method. The performance of Harris's, Lowe's, Tomasi's, Loupias's, and Yeh's methods are given in Figures 12(a), 12(b), 12(c), 12(d), and 12(e), respectively, for the same level of noise. The results demonstrate that except for Tomasi's technique, the other five methods work well in the presence of noise.

From the figures, it can be concluded that the proposed method can be used as an affine and scale invariant detector. To complement the subjective evaluations, we present a quantitative performance comparison of the proposed affine and scale invariant detector and other detectors. The stability and accuracy of the detectors are evaluated using the repeatability criterion [34]. The repeatability score for a given pair of images is the percentage of corresponding
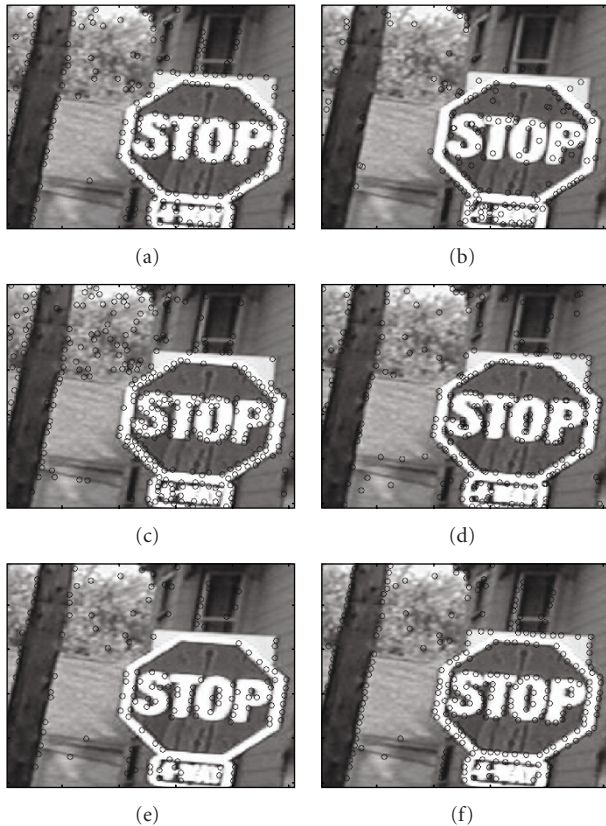
FIGURE 9: Feature points detected in 1.5 times scaled image by (a) Harris method (b) Lowe's method, (c) Tomasi's method, (d) Loupias's technique, (e) Yeh's algorithm, and (f) proposed technique.
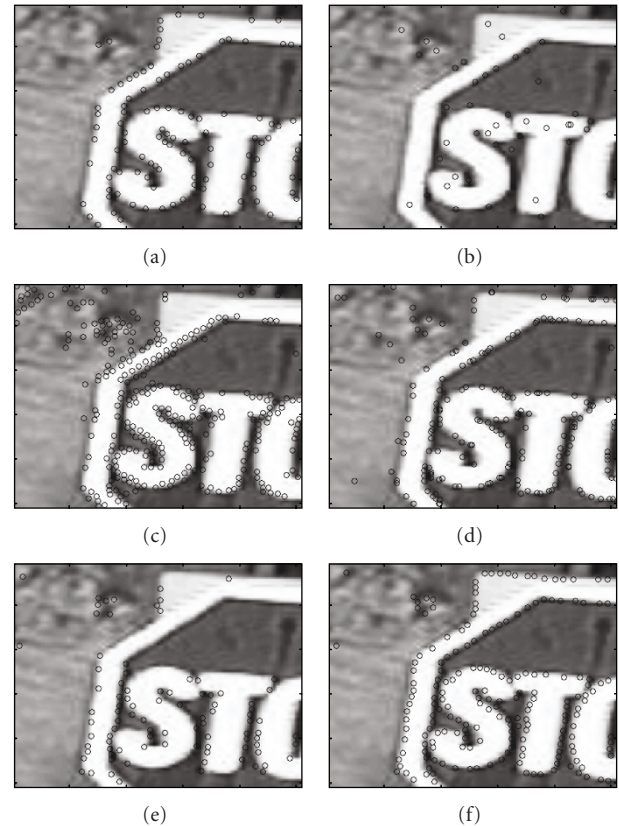

FIGURE 10: Feature points detected in 3.4 times scaled image by (a) Harris method (b) Lowe's method, (c) Tomasi's method, (d) Loupias's technique, (e) Yeh's algorithm, and (f) proposed technique.

points detected in those images under different geometric and photometric transformations. We take into account only the points located in the part of the scene present in both images. Measuring the repeatability rate within 1.5 pixels or less, the probability that two points are accidentally within the error distance is negligible.

We first compare the detectors for image rotation followed by scale change and additive noise. The repeatability rate as a function of the angle of image rotation is displayed in Figure 13(a). The rotation angles vary between $0°$ and $180°$. Under repeatability, Harris's and Lowe's methods give the best results for all rotations, where these algorithms obtain a repeatability rate of about 82% and 77%, respectively. From the observation of the plot of the repeatability rate with image rotation, the proposed technique does not outperform Harris method or SIFT algorithm, but it yields a repeatability rate of about 70% for all rotations. Notably, it offers better performance than Tomasi's, Loupious's, and Yeh's techniques, where these approaches offer a repeatability rate of about 60%, 50%, and 40%, respectively.

Figure 13(b) shows the repeatability rate as a function of scale changes. The results show that all the detectors are scale sensitive except Lowe's method. As the name implies, the SIFT algorithm proposed by Lowe offers the best performance with scale change. This method is the least

dependent on the change in scale. The Harris's, Tomasi's, and the proposed detectors give reasonable results, with the repeatability rate as a decreasing function of scale change. Laopious's and Yeh's methods are very sensitive to scale change and the results of these methods are hardly usable.

To study repeatability in the presence of image noise, the repeatability rate is displayed as a function of SNR. For performance evaluation with noise, the SNR is varied from 35 dB to 21 dB and the results are displayed in Figure 13(c). All the detectors give reasonable results in the additive noise cases, with the exception of Tomasi's method. Harris's and Laopious's methods give the best results followed by the proposed and then by Lowe's, Yeh's, and Tomasi's techniques. The proposed method obtains a repeatability rate of nearly 70% for all levels of noise considered.

For the evaluation of detection performance, the feature points extracted by the proposed method and the five other algorithms are presented for two more images in Figures 14 and 15, where the detected points are superimposed on the original image to evaluate the interest points location. From those figures, it is observed that the proposed method extract points where variations occur in the image, that is, where the image information is supposed to be the most important. Additionally, the set of detected interest points are not cluttered in a few regions rather spread out at different parts
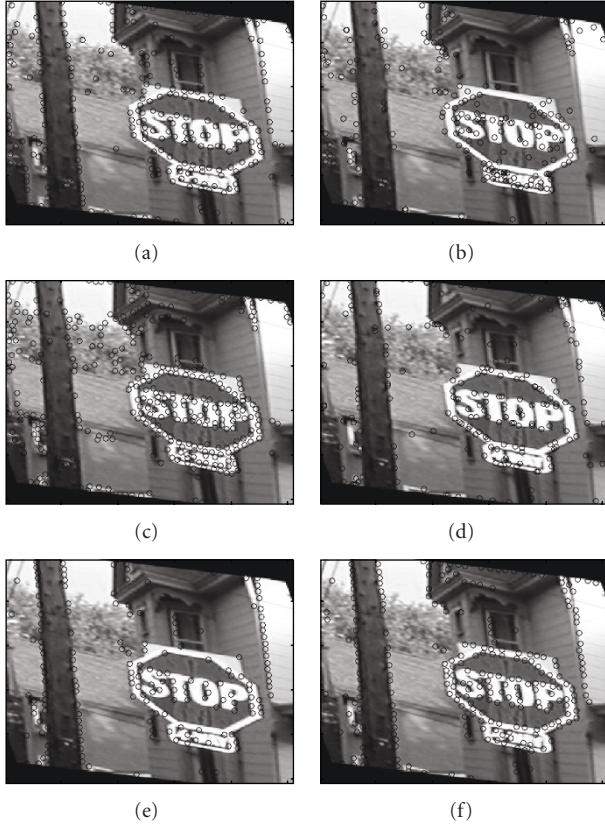
FIGURE 11: Feature points detected in sheared image by (a) Harris method (b) Lowe's method, (c) Tomasi's method, (d) Loupias's technique, (e) Yeh's algorithm, and (f) proposed technique.
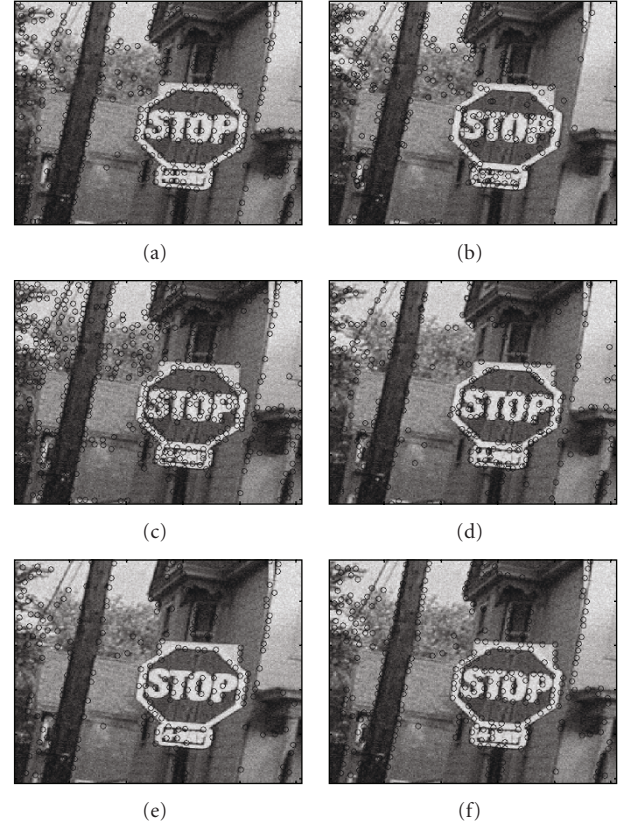

FIGURE 12: (a) Feature points detected in noisy image with SNR = 25 dB by (a) Harris method (b) Lowe's method, (c) Tomasi's method, (d) Loupias's technique, (e) Yeh's algorithm, and (f) proposed technique.

of the image. Most importantly, the proposed method covers all the curvatures of object boundaries and yields at the true features, that is, the edges, ridges, and corners. Accordingly, the extracted points detect the structure of the scene and lead to a complete image representation.

Analysis is done on the sensitivity to algorithm parameters. Most existing interest point detectors depend on the choice of some parameters. The threshold in Harris's method is chosen by trial and error depending on the problem at hand. The number of points detected by the SIFT algorithm varies significantly with the change in image intensity. For example, for the image used in the paper, the number of detected feature points by SIFT is 862, if the input image is not normalized and it is 363 if the same input image is normalized.

In the proposed method there is one threshold, th_z which determines the set of the first selection of the interest points such that any point will be selected if it exceeds a minimum number of zero crossings around it. This threshold is not a function of image intensity, rather it is the function of number of zero-crossing points of an IMF and thus, it is different for each edge segment of an image. In the paper, this threshold has been set as the 1/3 of the maximum number of zero crossings present in an IMF signal and this choice

is independent of the image. As this threshold selects the preliminary set of the feature points, any value which is equal to or smaller than the value yields the same result. Choosing the value for this threshold is not stringent and has minor effect on the final set of extracted feature points. Because the preliminary feature points selected by this threshold go through three more passes for the redundant points to be discarded. The two more thresholds in those passes define the size of the local neighborhood of a pixel. Thus, those thresholds are not a function of image intensity, but rather image size. The value of those two thresholds chosen in the paper work well for most of the images we come across in practice. We have tested Harris method and the proposed algorithm for different values of the threshold, th_z. Table 1 gives the number of detected points for Harris and the proposed method as a function of the threshold (th_z = Threshold × (1/3) of the maximum number of zero crossings).

After the examination of the overall detection results, it can be claimed that the proposed method compares favorably against other well-known methods. Based on the plot for the repeatability rate, the performance of the proposed technique is the least dependent on transformations and noise, which is a desirable and attractive characteristic for
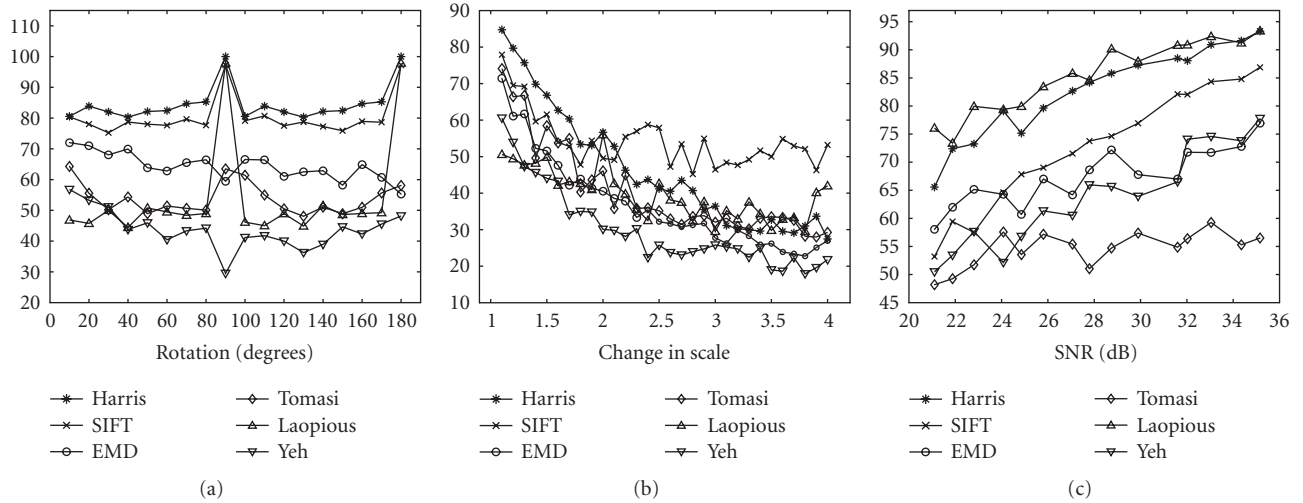
FIGURE 13: Plot for the repeatability rate as a function of (a) rotation angle, (b) change in scale, and (c) noise level.
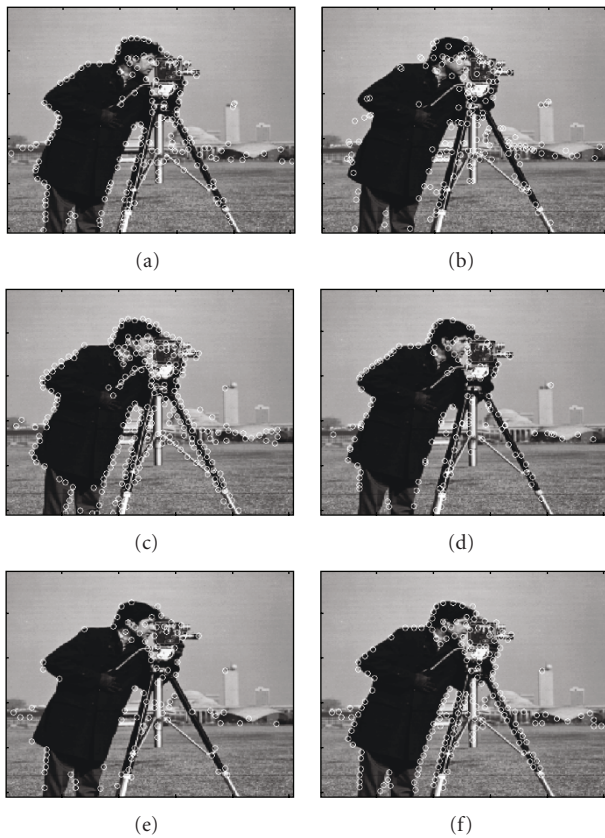

FIGURE 14: Feature points detected in the second image by (a) Harris method (b) Lowe's method, (c) Tomasi's method, (d) Loupias's technique, (e) Yeh's algorithm, and (f) proposed technique.
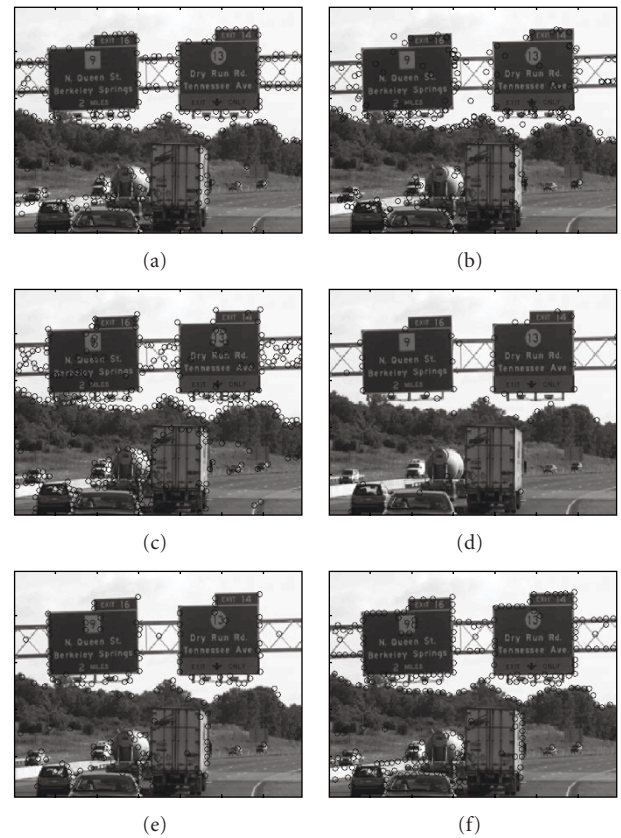

FIGURE 15: Feature points detected in the third image by (a) Harris method (b) Lowe's method, (c) Tomasi's method, (d) Loupias's technique, (e) Yeh's algorithm, and (f) proposed technique.

any feature point detector. Though the proposed technique does not outperform Harris method or SIFT algorithm, it yields better results than Tomasi's, Loupious's, and Yeh's techniques. Notably, it offers better performance than the other two contour-based methods: Loupious's and Yeh's approaches. Therefore, the proposed algorithm can be expected to perform well for applications where true interest points must correspond to image contours or object
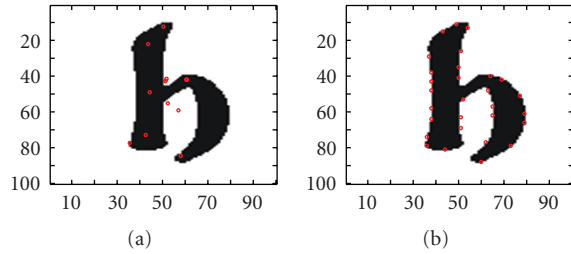
FIGURE 16: Interest points detected from the binary image of letter "h" by (a) the SIFT algorithm and (b) the proposed algorithm.

TABLE 1: Effect of threshold on the number of detected points.

Threshold	1	0.9	0.8	0.7	0.6	0.5	0.4	0.3	0.2	0.1
Harris method	303	308	314	322	326	334	346	362	377	391
Proposed method	303	303	303	303	303	303	303	303	303	303

boundaries for further processing. As an example, for a binary image, interest points should not be found in the uniform region of constant intensity, that is, either in the background or foreground. Rather interest points must lie only on the edges. As shown in Figure 16, for the binary image of the letter "h", the SIFT algorithm detects feature points in the uniform region. But the proposed method, as a contour-based technique, extracts interest points only from the edges, which signifies the performance variation of different algorithms depending on the types of image and/or applications.

4. CONCLUSION

This research presents a robust, rotation invariant, and scale-invariant corner detection scheme for images based on the morphological edge detection, the eigenvectors of covariance matrices for boundary segment points, and the 1D EMD. We modify an existing morphological edge detection scheme to yield thin edges and eliminat spurious edges resulting from the background. The main contribution of this work is the utilization of the first IMF of EMD of the 1D $\theta - P$ signal of the edge to localize true corner points on boundary contours. Under appropriate image resolution and region of support, the proposed approach precisely captures the true corner points and is free from false alarms on circular arcs for both simple and complicated objects in varying rotation, scale conditions, and noise contaminations.

The interesting attribute of this technique is that it does not detect feature points globally. Rather it detects feature points locally, based on the neighboring characteristics of a small edge segment. This results in the presented method being more independent of image transformation than the other five methods considered for comparison. Thus, interest points detected by the proposed method are largely independent of the imaging conditions; that is, detected points are geometrically stable.

Additionally, for the proposed technique we do not need either to implement the computational extensive 2D EMD or to calculate all the IMFs of 1D EMD. Only the first IMF of 1D EMD is required. Experimental results also suggest that the proposed 1D EMD-based corner detection approach is stable and efficient. The proposed method is a generic concept and can find its application in many matching and recognition problems.

REFERENCES

[1] A. Bandera, C. Urdiales, F. Arrebola, and F. Sandoval, "Corner detection by means of adaptively estimated curvature function," *Electronics Letters*, vol. 36, no. 2, pp. 124–126, 2000.

[2] R. Rattarangsi and R. T. Chin, "Scale-based detection of corners of planar curves," *IEEE Transactions on Pattern Analysis and Machine Intelligence*, vol. 14, no. 4, pp. 430–449, 1992.

[3] R. Horaud, F. Veillon, and T. Skordas, "Finding geometric and relational structures in an image," in *Proceedings of the 1st European Conference on Computer Vision (ECCV '90)*, pp. 374–384, Antibes, France, April 1990.

[4] E. Shilat, M. Werman, and Y. Gdalyahu, "Ridge's corner detection and correspondence," in *Proceedings of IEEE Computer Society Conference on Computer Vision and Pattern Recognition (CVPR '97)*, pp. 976–981, San Juan, Puerto Rico, USA, June 1997.

[5] F. Mokhtarian and R. Suomela, "Robust image corner detection through curvature scale space," *IEEE Transactions on Pattern Analysis and Machine Intelligence*, vol. 20, no. 12, pp. 1376–1381, 1998.

[6] A. Pikaz and I. Dinstein, "Using simple decomposition for smoothing and feature point detection of noisy digital curves," *IEEE Transactions on Pattern Analysis and Machine Intelligence*, vol. 16, no. 8, pp. 808–813, 1994.

[7] A. Bruce and H. Y. Gao, *Applied Wavelet Analysis with SPLUS*, Springer, New York, NY, USA, 1996.

[8] Y.-N. Sun, J.-S. Lee, and C. T. Tsai, "Multiscale corner detection by using wavelet transformation," *IEEE Transactions on Image Processing*, vol. 4, no. 4, pp. 100–104, 1995.

[9] C.-H. Chen, J.-S. Lee, and Y.-N. Sun, "Wavelet transformation for gray-level corner detection," *Pattern Recognition*, vol. 28, no. 6, pp. 853–861, 1995.

[10] A. Quddus and M. M. Fahmy, "Fast wavelet-based corner detection technique," *Electronics Letters*, vol. 35, no. 4, pp. 287–288, 1999.

[11] A. Quddus and M. Gabbouj, "Wavelet-based corner detection technique using optimal scale," *Pattern Recognition Letters*, vol. 23, no. 1–3, pp. 215–220, 2002.

[12] J. P. Hua and Q. M. Liao, "Wavelet-based multi scale corner detection," in *Proceedings of the 5th International Conference on Signal Processing (ICSP '00)*, pp. 341–344, Beijing, China, August 2000.

[13] E. Loupias, N. Sebe, S. Bres, and J.-M. Jolion, "Wavelet-based salient points for image retrieval," in *Proceedings of IEEE International Conference on Image Processing (ICIP '00)*, vol. 2, pp. 518–521, Vancouver, BC, Canada, September 2000.

[14] M. S. Lew, E. Loupias, T. S. Huang, Q. Tian, and N. Sebe, "Image retrival using wavelet-based salient points," *Journal of Electronic Imaging*, vol. 10, no. 4, pp. 835–849, 2001.

[15] C.-H. Yeh, "Wavelet-based corner detection using eigenvectors of covariance matrices," *Pattern Recognition Letters*, vol. 24, no. 15, pp. 2797–2806, 2003.

[16] K. Rohr, "Recognizing corners by fitting parametric models," *International Journal of Computer Vision*, vol. 9, no. 3, pp. 213–230, 1992.

[17] R. Deriche and T. Blaszka, "Recovering and characterizing image features using an efficient model based approach," in *Proceedings of IEEE Computer Society Conference on Computer Vision and Pattern Recognition (CVPR '93)*, pp. 530–535, New York, NY, USA, June 1993.

[18] S. Baker, S. K. Nayar, and H. Murase, "Parametric feature detection," *International Journal of Computer Vision*, vol. 27, no. 1, pp. 27–50, 1998.

[19] L. Parida, D. Geiger, and R. Hummel, "Junctions: detection, classification, and reconstruction," *IEEE Transactions on Pattern Analysis and Machine Intelligence*, vol. 20, no. 7, pp. 687–698, 1998.

[20] H. P. Moravec, "Towards automatic visual obstacle avoidance," in *Proceedings of the 5th International Joint Conference on Artificial Intelligence (IJCAI '77)*, p. 584, Cambridge, Mass, USA, August 1977.

[21] P. R. Beaudet, "Rotationally invariant image operators," in *Proceedings of the 4th International Joint Conference on Pattern Recognition (ICPR '78)*, pp. 579–583, Kyoto, Japan, November 1978.

[22] L. Kitchen and A. Rosenfeld, "Gray-level corner detection," *Pattern Recognition Letters*, vol. 1, no. 2, pp. 95–102, 1982.

[23] W. Förstner, "A framework for low level feature extraction," in *Proceedings of the 3rd European Conference on Computer Vision (ECCV '94)*, pp. 383–394, Stockholm, Sweden, May 1994.

[24] C. Harris and M. Stephens, "A combined corner and edge detector," in *Proceedings of the 4th Alvey Vision Conference (AVC '88)*, pp. 147–151, Manchester, UK, September 1988.

[25] C. Tomasi and T. Kanade, "Detection and tracking of point features," Tech. Rep. CMU-CS-91-132, Carnegie Mellon University, Pittsburgh, Pa, USA, 1991.

[26] J. Shi and C. Tomasi, "Good features to track," in *Proceedings of IEEE Computer Society Conference on Computer Vision and Pattern Recognition (CVPR '94)*, pp. 593–600, Seattle, Wash, USA, June 1994.

[27] F. Heitger, L. Rosenthaler, R. von der Heydt, E. Peterhans, and O. Kübler, "Simulation of neural contour mechanism: from simple to end-stopped cells," *Vision Research*, vol. 32, no. 5, pp. 963–981, 1992.

[28] S. M. Smith and J. M. Brady, "SUSAN—a new approach to low level image processing," *International Journal of Computer Vision*, vol. 23, no. 1, pp. 45–78, 1997.

[29] R. Laganiere, "Morphological corner detection," in *Proceedings of the 6th IEEE International Conference on Computer Vision (ICCV '98)*, pp. 280–285, Bombay, India, January 1998.

[30] D. G. Lowe, "Distinctive image features from scale-invariant keypoints," *International Journal of Computer Vision*, vol. 60, no. 2, pp. 91–110, 2004.

[31] N. E. Huang, Z. Shen, S. R. Long, et al., "The empirical mode decomposition and the Hilbert spectrum for nonlinear and non-stationary time series analysis," *Proceedings of the Royal Society A*, vol. 454, no. 1971, pp. 903–995, 1998.

[32] K.-K. Chin and J. Saniie, "Morphological processing for feature extraction," in *Image Algebra and Morphological Image Processing IV*, vol. 2030 of *Proceedings of SPIE*, pp. 288–302, San Diego, Calif, USA, July 1993.

[33] D.-M. Tsai, H.-T. Hou, and H.-J. Su, "Boundary-based corner detection using eigenvalues of covariance matrices," *Pattern Recognition Letters*, vol. 20, no. 1, pp. 31–40, 1999.

[34] C. Schmid, R. Mohr, and C. Bauckhage, "Evaluation of interest point detectors," *International Journal of Computer Vision*, vol. 37, no. 2, pp. 151–172, 2000.

[35] J. Canny, "A computational approach to edge detection," *IEEE Transactions on Pattern Analysis and Machine Intelligence*, vol. 8, no. 6, pp. 679–698, 1986.

[36] S. Sinclair and G. G. S. Pegram, "Empirical mode decomposition in 2-D space and time: a tool for space-time rainfall analysis and nowcasting," *Hydrology and Earth System Sciences*, vol. 9, no. 3, pp. 127–137, 2005.

[37] J. Serra, *Image Analysis and Mathematical Morphology*, Academic Press, New York, NY, USA, 1982.

[38] S. U. Lee, S. Y. Chung, and R. H. Park, "A comparative performance study of several global thresholding techniques for segmentation," *Computer Vision, Graphics and Image Processing*, vol. 52, no. 2, pp. 171–190, 1990.

[39] D. Marr and E. Hildreth, "Theory of edge detection," *Proceedings of the Royal Society of London B*, vol. 207, no. 1167, pp. 187–217, 1980.

[40] X. Chen, J. Yang, J. Zhang, and A. Waibel, "Automatic detection and recognition of signs from natural scenes," *IEEE Transactions on Image Processing*, vol. 13, no. 1, pp. 87–99, 2004.

[41] A. K. Jain and B. Yu, "Automatic text location in images and video frames," *Pattern Recognition*, vol. 31, no. 12, pp. 2055–2076, 1998.

[42] V. Kastrinaki, M. Zervakis, and K. Kalaitzakis, "A survey of video processing techniques for traffic applications," *Image and Vision Computing*, vol. 21, no. 4, pp. 359–381, 2003.

[43] Y. M. Y. Hasan and L. J. Karam, "Morphological text extraction from images," *IEEE Transactions on Image Processing*, vol. 9, no. 11, pp. 1978–1983, 2000.

[44] H. Liang, Q.-H. Lin, and J. D. Z. Chen, "Application of the empirical mode decomposition to the analysis of esophageal manometric data in gastroesophageal reflux disease," *IEEE Transactions on Biomedical Engineering*, vol. 52, no. 10, pp. 1692–1701, 2005.

[45] D. Rouvre, D. Kouamé, F. Tranquart, and L. Pourcelot, "Empirical mode decomposition (EMD) for multi-gate, multi-transducer ultrasound Doppler fetal heart monitoring," in *Proceedings of the 5th IEEE International Symposium on Signal Processing and Information Technology (ISSPIT '05)*, pp. 208–212, Athens, Greece, December 2005.

[46] Z. Liu, H. Wang, and S. Peng, "Texture classification through directional empirical mode decomposition," in *Proceedings of the 17th International Conference on Pattern Recognition (ICPR '04)*, vol. 4, pp. 803–806, Cambridge, UK, August 2004.

[47] Md. K. I. Molla and K. Hirose, "Single-mixture audio source separation by subspace decomposition of Hilbert spectrum," *IEEE Transactions on Audio, Speech and Language Processing*, vol. 15, no. 3, pp. 893–900, 2007.

[48] T. Zhu, "Suspicious financial transaction detection based on empirical mode decomposition method," in *Proceedings of IEEE Asia-Pacific Conference on Services Computing (APSCC '06)*, pp. 300–304, Guangzhou, China, December 2006.

[49] R. C. Gonzalez and R. E. Woods, *Digital Image Processing*, Addison Wesley, Reading, Mass, USA, 1993.